Biosensors and Bioelectronics 53 (2014) 513–518

Contents lists available at ScienceDirect

Biosensors and Bioelectronics

journal homepage: www.elsevier.com/locate/bios

Au nanoparticle-modified DNA sensor based on simultaneous electrochemical impedance spectroscopy and localized surface plasmon resonance

Xin R. Cheng [a], Ben Y.H. Hau [a], Tatsuro Endo [b], Kagan Kerman [a,*]

[a] Department of Physical and Environmental Sciences, University of Toronto Scarborough, 1265 Military Trail, Toronto, ON, Canada M1C 1A4
[b] Department of Applied Chemistry, Osaka Prefecture University, 1-1 Gakuen-cho, Naka-ku, Sakai-shi, Osaka, Japan

ARTICLE INFO

Article history:
Received 14 July 2013
Received in revised form
27 September 2013
Accepted 4 October 2013
Available online 17 October 2013

Keywords:
Au nanoparticles
Electrochemical impedance spectroscopy
Localized surface plasmon resonance
DNA hybridization
Electrodeposition
Apolipoprotein E

ABSTRACT

Electrochemical impedance spectroscopy (EIS) and localized surface plasmon resonance (LSPR) were performed on the same Au nanoparticle (AuNP)-modified indium tin oxide (ITO) coated glass surfaces. Cyclic voltammetry was applied to electrodeposit AuNPs on ITO surface directly. The surface plasmon band characterization of AuNPs was initially studied by controlling the electrodeposition conditions. It was found that the size of AuNP clusters was significantly affected by the applied potential and KCl concentration in solution. The dual-detection platform was applied to detect DNA hybridization related to a specific point mutation in apolipoprotein E gene (ApoE), which was related to the progression of Alzheimer's disease. The preliminary results facilitate the development of a versatile biosensor that can be easily miniaturized and integrated into a high-throughput diagnostic device.

1. Introduction

Indium tin oxide (ITO) is a unique material that has been used extensively in sensor applications due to its prominent characteristics such as excellent optical transparency, wide working potential, high electrical conductivity, substrate adhesion and stability (Lahav et al., 1999; Cheng et al., 2002; Lee et al., 2003; Toyota et al., 2004). ITO was utilized in this report as the sensing platform for localized surface plasmon resonance (LSPR) and electrochemical impedance spectroscopy (EIS) measurements. Noble metal nanoparticles exhibit rich LSPR properties, which result from the collective oscillation of conductive electrons in response to excitation by light (Haes and Van Duyne, 2004; Murphy et al., 2009). The intensity of LSPR was determined to be highly sensitive to dielectric properties such as refractive index (RI) of molecules close to the nanoparticle surface. This discovery has led to the proliferation of Au nanoparticles (AuNPs) as biosensors in various applications (Endo et al., 2005, 2006, 2007, 2008; Haes and Van Duyne, 2002; Kim et al., 2007). Furthermore, since LSPR sensing is based on a simple optical extinction measurement, it can be readily miniaturized to nanosensors (Anker et al., 2008). The Kretschmann configuration of the classical SPR requires a glass body with evaporated gold and the evanescent wave detects refractive changes on Au film surface. The major advantage of LSPR over the conventional SPR is its cost-effectiveness and simplicity, as the measurements can be performed at a single wavelength in a transmission configuration using a UV–vis spectrophotometer (Anker et al., 2008).

Electrochemical impedance spectroscopy (EIS) has seen tremendous increase in popularity in recent years (Long et al., 2004; Paleček and Bartošík, 2012; Randviir and Banks, 2013; Chang and Park, 2010; Liang et al., 2013). EIS depicts the system response to the application of a periodic small amplitude alternating current signal. In EIS-based DNA sensor studies, the impedance of an electrode undergoing heterogeneous electron transfer through a self-assembled film of DNA can be described using an equivalent circuit comprising capacitance and resistance elements such as R_s (solution resistance), R_{CT} (charge transfer resistance), CPE (constant phase element) and the mass transfer element W (Warburg impedance). A common strategy is to use an indicator, such as ferri–ferrocyanide ($[Fe(CN)_6]^{3-/4-}$) redox couple. Formation of a mismatched duplex results in considerable amount of changes in the electrical properties of the DNA film on the electrode surface as detected by Nyquist plots. These plots are then analyzed commonly by using Randle's equivalent circuit. In this report, EIS was employed to serve as a confirmation of the LSPR results using the same DNA sensor.

Although some recently reported LSPR-based DNA sensors had fairly low detection limits (Hiep et al., 2008a, 2008b), the fabrication process was not cost- and labor-effective. A melittin sensor

* Corresponding author. Tel.: +1 416 287 7250.
E-mail address: kagan.kerman@utoronto.ca (K. Kerman).

0956-5663/$ - see front matter © 2013 Elsevier B.V. All rights reserved.
http://dx.doi.org/10.1016/j.bios.2013.10.003

based on dual detection platform employing LSPR and EIS on an ITO electrode required a tedious fabrication procedure that would take days to complete (Hiep et al., 2008a, 2008b). Therefore, in this work, we aim to design a simple and novel fabrication method. DNA films were prepared on AuNPs that were electrodeposited on an ITO surface. The size and distribution of AuNP clusters were controlled by varying the applied potential, solution conditions and electrodeposition time.

As a proof-of-concept study, apolipoprotein E (ApoE) gene was detected on the dual-detection platform. ApoE is an essential constituent of several plasma lipoproteins (de Bellis et al., 1997). It is present in three isoforms (E2, E3 and E4) and related to two polymorphic codon sites (112 and 158) of the gene located on chromosome 19. Polymorphisms of ApoE influence a variety of neuropathological processes (Corder et al., 1993; Farrer et al., 1997; Morris et al., 2010). Recent studies have shown that the inheritance of one or more mutations increases an individual's risk of developing type-III hyperlipidemia, atherosclerosis and Alzheimer's disease (Venter, 2001). Various electrochemical DNA sensors have been developed for the detection of ApoE gene mutations (Marrazza et al., 2000, 2001; Ahmed et al., 2007; Guo et al., 2011). To the best of our knowledge, this is the first report that describes a simple DNA biosensing platform that enables EIS and LSPR measurements on the same ITO surface as illustrated in Scheme 1.

2. Experimental

2.1. Reagents

Oligonucleotides were purchased from BioBasic, Inc. (Markham, ON). The probe was a 5′-disulfide-hexane modified 23 base-pairs (bp) long oligonucleotide from a fragment of the allele-3 around codon-158 that contained a point mutation (underlined in the mismatch (MM) sequence) with reported links to the progression of Alzheimer's disease (Venter, 2001).

Probe:
5′-ACC TGC AGA AGC GCC TGG CAG TG-3′

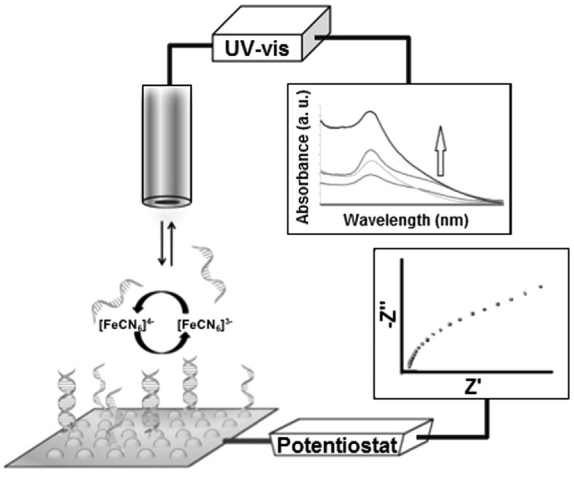

Scheme 1. Illustration of the DNA sensor with dual-detection platform for LSPR and EIS measurements. DNA probes were immobilized on the AuNP-modified ITO surface as the biorecognition layer. After the hybridization with the target oligonucleotides, EIS was measured using $[Fe(CN)_6]^{3-/4-}$ as the solution-based electro-active indicator. Simultaneously, LSPR was detected using a microfiber bundle in connection with a miniaturized UV–vis spectrophotometer .

Target (T):
5′-CAC TGC CAG GCG CTT CTG CAG GT-3′
Mismatch (MM):
5′-CAC TGC CAG GC**A** CTT CTG CAG GT-3′
Non-Complementary (NC):
5′-GAT TAG AGT CCC GCA ATT AAT CAT T-3′

The stock solution of thiolated probes was prepared using the immobilization buffer (1 M KH_2PO_4, pH 3.80). Hybridization buffer included 20 mM Na_2HPO_4 with 300 mM NaCl and 100 mM EDTA at pH 7.40. ITO-coated glass substrates (1 mm thickness) were fabricated in our laboratory. All other chemicals were of analytical grade, and were obtained from Sigma-Aldrich (Oakville, ON), unless otherwise specified.

2.2. Electrodeposition of AuNPs on ITO surface

A custom-made electrochemical cell was used to house the modified ITO substrates, and a conventional three-electrode arrangement was used. A coiled platinum wire served as an auxiliary electrode with the Ag/AgCl reference electrode from CH Instruments Inc. (Austin, TX). ITO substrates were cut and cleaned ultrasonically with dilute ammonia, ethanol and deionized water for 3 min. The substrates were then immersed into a solution of 100 nM $HAuCl_4$ in 100 mM phosphate buffer solution with varying concentrations of KCl. Cyclic voltammetry (CV) was conducted under ambient conditions using the CHI440A electrochemical workstation (CH Instruments, Inc. Austin, TX). The potential range was kept constant for all recordings from −1.00 to 1.15 V vs. Ag/AgCl, with a scan rate of 100 mV/s. All LSPR and EIS measurements were performed in replicates using different surfaces from repetitive electrodeposition experiments.

2.3. Scanning electron microscopy (SEM)

SEM of AuNPs on ITO surfaces was performed using a Hitachi S530 scanning electron microscope (Hitachi, Japan). All ITO chips were Au sputtered using the SEM coating unit PS3 (Agar Scientific) at 19 mA plasma current for 100 s. The chips were then electrically connected to the sample stub by smearing silver paste dissolved in acetone from the sample to the metallic stub. The surface was observed at an acceleration voltage of 20 kV with a working distance of 5.0 mm. Hitachi S-5200 SEM was used for high resolution images; the ITO chips were adhered to SEM stubs by conductive carbon paint (SPI Supplies, West Chester, PA, USA). The electron gun voltage was set at 5.0 kV and the software used to view the SEM images was Quartz PCI (Quartz Imaging Corporation, Vancouver, BC). The thickness of the Au-sputtered layer was calculated using the procedure described by Merrick et al. (1973). ImageJ (US National Institutes of Health, MD) was subsequently used to determine the size distribution of the AuNP deposited surfaces. Results are described in the Supplementary information.

2.4. DNA immobilization on AuNP-modified ITO surfaces

The probe immobilization efficiency was first optimized by concentration studies. Probe oligonucleotides were spotted on the AuNP-modified ITO surfaces in the immobilization buffer. To remove the non-specifically adsorbed species, these surfaces were incubated in a moist environment for 4 h, and then rinsed with PBS. After the immobilization of the probe on the surface, target oligonucleotides were exposed to the surface for 2 h. After rinsing with PBS, LSPR and EIS measurements were recorded before and after each modification of the ITO surfaces with biomolecules.

2.5. Localized surface plasmon resonance (LSPR)

LSPR setup comprised a spectrophotometer (USB-4000-UV–vis), a tungsten halogen light source (LS-1-LL, wavelength range 200–1100 nm), a fiber probe bundle (fiber core diameter 400 μm, wavelength range 300–1100 nm) and WS-1 diffuse reflectance standard that were purchased from Ocean Optics (Dunedin, FL). All measurements were standardized using a blank ITO on a white platform, with a constant probe height to the sample. All data gathered by the LSPR setup were compiled and analyzed using the Spectral Suite software (Ocean Optics, Dunedin, FL).

DNA sensing using LSPR was conducted using a similar setup to the one that was used to detect the presence of AuNPs. White light emerging from the optical fiber bundle was incident onto the AuNP layer substrate from the vertical direction. All absorbance spectra were taken from 400 to 800 nm at room temperature.

2.6. Electrochemical impedance spectroscopy (EIS) and cyclic voltammetry

EIS was conducted using the Metrohm Autolab PGSTAT302N (Metrohm, Switzerland) in connection with a home-made electrochemical cell placed in a grounded Faraday cage. Unlike in CV electrodeposition, the ITO substrate was clamped between O-rings such that the surface area of the substrate exposed to the supporting electrolyte solution was fixed at 2 cm^2. All impedance measurements had an applied potential of 0.25 V (vs. Ag/AgCl) for the redox probe 10 mM $[Fe(CN)_6]^{3-/4-}$. The amplitude voltage was 5 mV and frequency ranged from 100 kHz to 100 mHz. All EIS data were computed by the Autolab Frequency Response Analyzer (FRA) software to produce Nyquist plots. CV was carried out at room temperature with a scan range from −1.00 V to 1.15 V, at 0.1 V/s with a step potential of 5 mV in the presence of

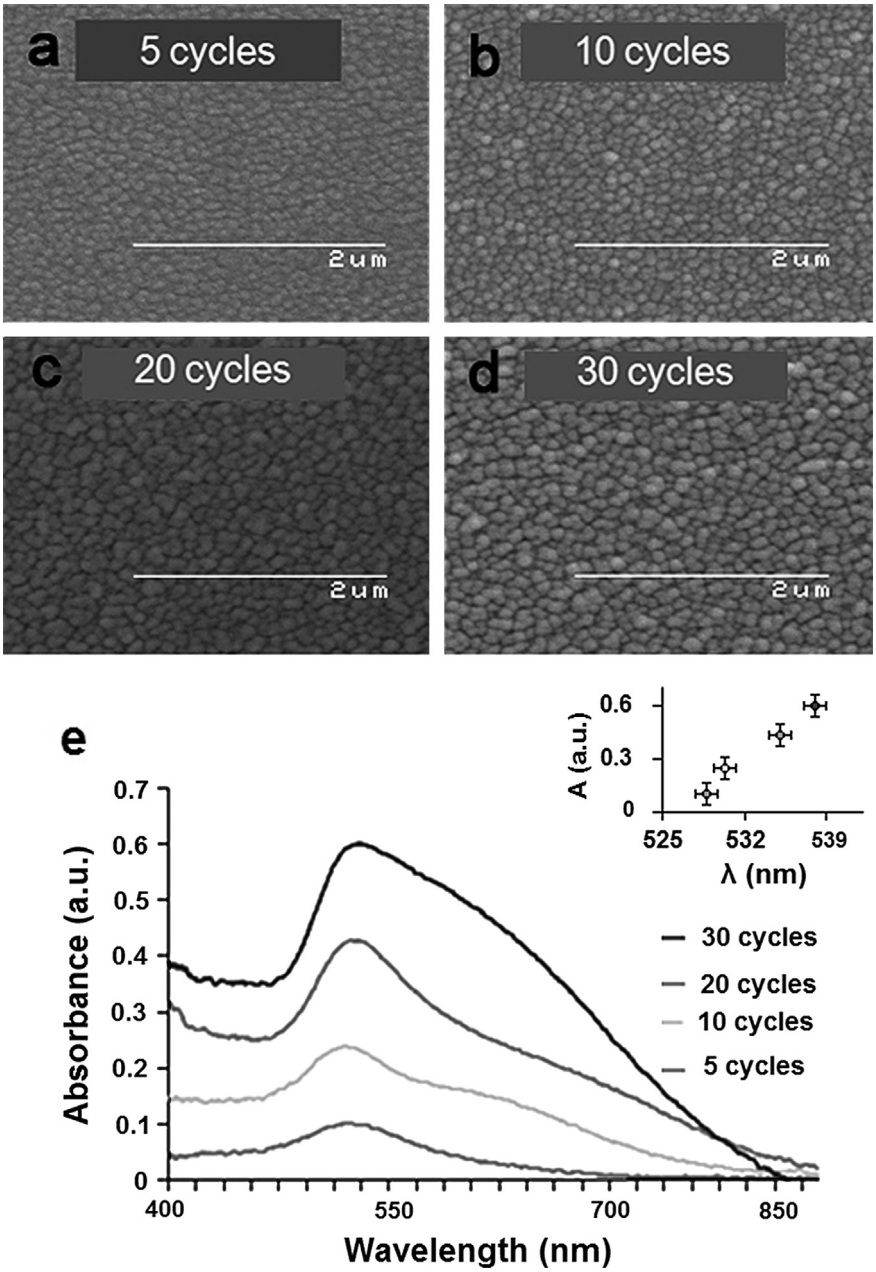

Fig. 1. SEM images of AuNPs electrodeposited on ITO surface for (a) 5 cycles, (b) 10 cycles, (c) 20 cycles, and (d) 30 cycles of CV. (e) LSPR band intensity of AuNPs on ITO surface increased with the increasing number of CV scans from −1.0 to 1.1 V at a scan rate of 0.1 V/s. Inset displays the effect of CV cycles on the red-shift and LSPR response of the AuNPs on ITO surface with no KCl in solution.

10 mM $[Fe(CN)_6]^{3-/4-}$. All LSPR and EIS measurements were performed in replicates ($n \geq 3$). The detection limits of both LSPR and EIS were calculated using the formula LOD = 3.3(SD/S), where SD represents the standard deviation of response and S represents the slope of calibration curve.

3. Results and discussion

AuNPs were electrodeposited on the surface of ITO glass substrates using a one-step and non-templated cyclic voltammetric procedure. First, the nucleation and growth steps were optimized in order to prepare the layer of AuNPs on the surface. At potentials lower than −0.50 V, nucleation with a sufficiently large overpotential could be achieved to seed the surface with nuclei of AuNP at the first CV cycle, and then the growth of AuNPs continued in subsequent cycles. In this report, a lower limit potential of −1.00 V was applied (Fig. S1). The higher limit potential was also increased to 1.15 V, so that small aggregates would be dissolved in the anodic process. In comparison with our electrodeposition technique, there were significant differences in the morphology and size of the nanoparticles in literature due to their varying fabrication process. For example, in the study by Ma et al. (2009), a narrower potential window (e.g. −1.1 V to −0.3 V) for the CV scans was used, which led to smaller and lower density AuNPs formation. In the work performed by Hezard et al. (2012), the electrodeposition process was performed entirely in the positive potential range against Ag/AgCl in sodium nitrate solution to form smaller AuNPs of ~36 nm on glassy carbon electrode surfaces. Au nanorods were also formed using chemical vapor deposition of Au onto anodic alumina layer with pores 20 nm in diameter (Claussen et al., 2011). Despite the high uniformity of this technique, the chip fabrication process was expensive and time consuming. Overall, the electrodeposition technique described in this study demonstrated a simple and cost-effective system to fabricate large AuNPs on ITO surfaces.

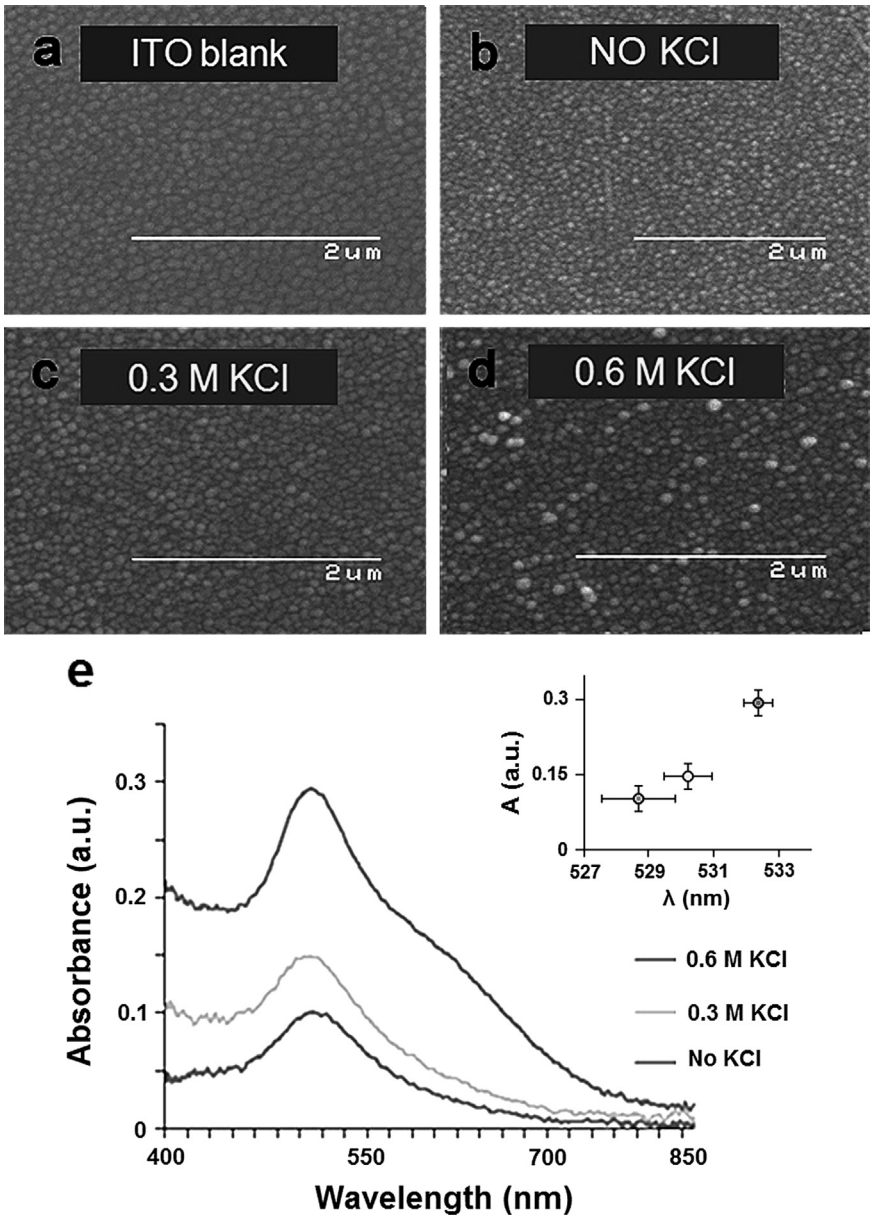

Fig. 2. SEM images of (a) a blank ITO surface, (b) AuNP-modified ITO surface with 5 cycles of CV scans in no KCl, and in the presence of KCl at (c) 0.3 M and (d) 0.6 M. (e) LSPR spectra of AuNPs on ITO indicated the enhancement of the signal at ~530 nm with increasing KCl concentrations. Other experimental conditions were as described in Fig. 1. Inset displays the effect of KCl concentration on the red-shift and LSPR response of the AuNP-modified ITO surface prepared with five CV cycles.

The size of the electrodeposited AuNPs was mostly between 50 and 80 nm (Fig. S2). As the number of CV cycles increased, more nuclei were seeded on the surface. This was supported by the size distribution graphs produced by imageJ analysis (Fig. S3A). As shown in Fig. 1, the AuNP morphology of 5 cycles did not vary significantly from those of more cycles. However, it could be seen that as the cycle numbers increased, LSPR response increased accordingly (Fig. 1(e)). As cycle numbers increased to 30, large aggregates started to form. We have performed the morphology and size distribution analysis of electrodeposition replicates using the software imageJ and found that the nanostructure sizes on surfaces from different sets of repeated experiments were statistically similar (Fig. S3A).

High resolution SEM images also displayed that the AuNP clusters increased in size as the amount of cycle numbers increased. The gold sputtering did not alter the morphology of the AuNP-modified surfaces considerably and was in fact found useful to enhance the SEM imaging of the surfaces (Fig. S2).

The effect of KCl concentration was also studied on AuNP-modified ITO substrates prepared with 5 cycles of CV scans. As shown in Fig. 2(a)–(d), it was observed that the AuNP size increased with increasing KCl in the electrolyte. However, there was no apparent change in shape of the AuNP clusters, as they still looked quasispherical when electrodeposition was performed in the presence of 600 mM KCl concentration. The size increase was consistent with the reported literature (Wang et al., 2008, 2009) and supported by imageJ analysis (Fig. S3B). The red color of AuNP-modified ITO surface was visible to the naked eye, and UV–vis spectra of the surfaces prepared with different CV cycles and KCl concentrations were investigated as well. The peak wavelength obtained after 5 cycles of CV in the absence of KCl was 528.7 ± 1.2 nm with an intensity of 0.1 ± 0.03 a.u. (Fig. 2 inset). It was observed that the effect of CV cycles on the electrodeposition resulted in an increase in LSPR intensity as well as a red-shift in wavelength. This observation was supported by Murphy et al. (2009), as they increased the electrodeposition time for AuNPs on ITO. It could also be observed that there was a shoulder peak emerging at 30 CV cycles (Fig. 1(e)). This result was attributed to an increase in the aspect ratio of the AuNP formed (Willets and Van Duyne, 2007). The presence of KCl also resulted in an increase in intensity and peak wavelength red-shift in the LSPR signal (Fig. 2(e)). Interestingly, the shoulder peak was not as apparent as the one recorded after 30 cycles of CV, which was attributed to the small change in the aspect ratio of AuNPs at 600 mM KCl. Eventually, the AuNP-modified ITO surfaces prepared with 30 cycles of CV in the presence of 600 mM KCl were utilized for the following experiments.

As shown in Fig. 3(a), a distinct shift in peak wavelength was observed after the immobilization of probe onto the AuNP modified ITO surface. The effective thickness of the adsorbate layer and electromagnetic decay length also affected the spectral shift of the system (Anker et al., 2008). This implied an increased wavelength shift was resulted from the binding of more or larger molecules on the surface. Similar effects of increased intensity and red-shift of LSPR peaks by molecular binding on the surface of AuNPs were observed in previously reported biosensor applications (Hsu et al., 2011; Endo et al., 2010; Hiep et al., 2010). LSPR signal increased in a concentration-dependent manner as target DNA (T) hybridized with the probe. The shifts in the peak wavelength were, however, negligible, which was attributed to the similar film properties on the AuNP (Fig. S4a). The detection limit was determined to be 512 nM (Fig. S5). It was also shown in Fig. 3(b) that a mismatch oligonucleotide (MM) could be distinguished from the fully complementary target (T). The exposure of a non-complementary (NC) oligonucleotide to the probe surface did not cause any significant LSPR change after wash. The non-linearity of the increase in the LSPR signal after the addition of MM oligonucleotides is in agreement with Kim et al. (2007). This phenomenon was attributed to the collective effect of the mismatched oligonucleotides, which might have produced structurally disruptive kinks after binding to the probe, to create steric hindrance that prevented more MM oligonucleotides from binding.

Statistical tests were performed, and the two-tailed p value was found to be 0.0161 for the hybridization of probe with MM and probe with T, and 0.0028 for the hybridization of probe with an NC and probe with T. By using the conventional criteria of $p < 0.05$, these differences were considered to be significant.

The proposed equivalence circuit that was applied in EIS measurements is shown in the inset of Fig. 4. R_s, which represents the resistance of the electrolyte solution, is determined by the electrolyte concentration. C_{dl} represents the double layer capacitance of the external AuNPs/electrolyte interface, and R_{CT} is the charge-transfer resistance related to the process of $[Fe(CN)_6]^{3-/4-}$ redox. This value was important in the evaluation of the impeding layer on AuNP-modified ITO surfaces. C_f is the capacitance of the AuNPs/solution interface, and R_f represents the resistance that develops between the AuNPs and the ITO surface (Grodzka et al., 2009). CV scans of the 10 mM $[Fe(CN)_6]^{3-/4-}$ couple shown in Fig. S6 were also used to confirm EIS results.

A concentration dependence study of hybridization was performed on the probe immobilized surfaces. As shown in Fig. S7a, R_{CT} calculated from the simulated model increased as the concentration of T oligonucleotide incubated increased. Nyquist plots showed an increase in 'semi-circle' diameter with the increase in target DNA concentration corresponding to the increase in R_{CT} (Fig. S7). The detection limit for T DNA was determined to be 286 nM using the EIS technique.

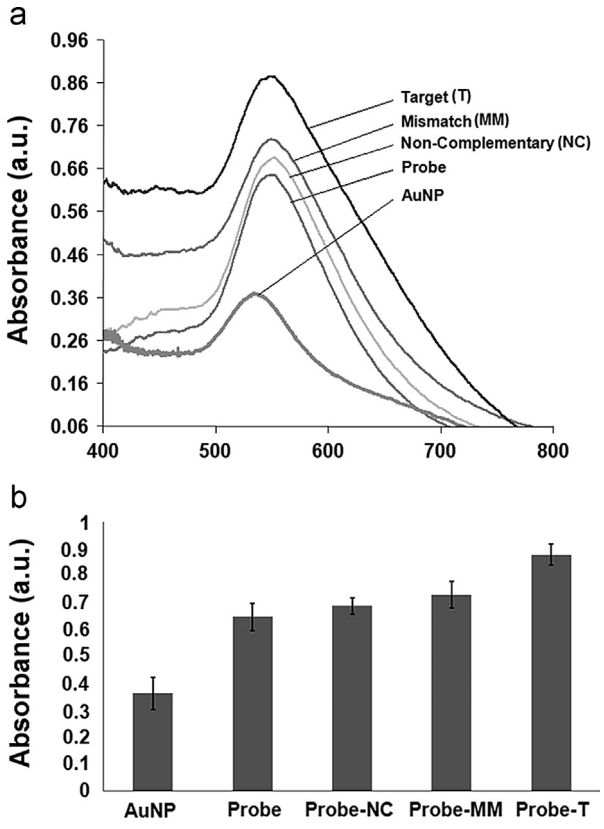

Fig. 3. (a) LSPR signals recorded for each hybridization event with the probe oligonucleotides on the AuNP-modified ITO surface. (b) Graph for the relative changes in LSPR responses obtained after modification of the AuNP-modified ITO surface with different oligonucleotides. Error bars indicate the standard deviation of triplicate measurements ($n=3$).

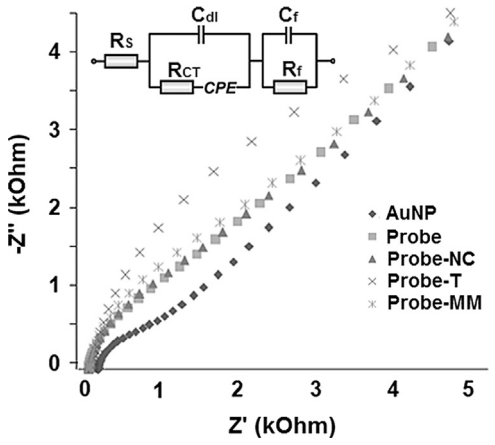

Fig. 4. Representative Nyquist plots recorded for the hybridization of various oligonucleotides with the probe immobilized on AuNP-modified ITO.

Table 1
Charge transfer resistance (R_{CT}) and the double-layer capacitance (C_{dl}) values for respective surface modifications on ITO glass substrates.

	R_{CT} (kΩ)	C_{dl} (μF)
AuNP	0.525 ± 0.033	6.09 ± 0.51
AuNP+P	0.828 ± 0.059	6.73 ± 0.48
AuNP+P+NC	1.073 ± 0.109	6.95 ± 0.26
AuNP+P+MM	1.705 ± 0.231	7.36 ± 0.18
AuNP+P+T	4.373 ± 0.268	14.47 ± 0.45

As shown in Table 1 and Fig. 4, the R_{CT} values increased after the immobilization process and subsequent oligonucleotide hybridization. The increase in R_{CT} after hybridization of T DNA was more than 5 times of the immobilized probe R_{CT} itself. MM and NC DNA could also be easily distinguished from T DNA. The R_{CT} values were correlated with the LSPR data for all the conditions described. The correlation coefficient calculated was 0.792, showing a good correlation between LSPR and EIS data, supporting the claim of a dual detection platform fabricated using simple electrodeposition of AuNP on an ITO surface.

4. Conclusions

The fabrication of AuNPs on the ITO surfaces required only one-step electrodeposition. The proof-of-concept study resulted in the detection limits of 512 nM and 286 nM of target oligonucleotides using LSPR and EIS techniques, respectively. Using this DNA sensor, MM and NC sequences could be directly discriminated from complementary DNA facilitating the development of future diagnostic studies for Alzheimer's disease. ApoE gene tests are commonly done using PCR from cheek swabs or blood samples of actual patients. After 30 cycles the gene content increases 9 magnitudes in concentration to amounts that can then be easily detected with enzyme cleaving and gel electrophoresis. Other ApoE sensors in the literature used a combination of PCR and piezoelectric technique to detect 2 μM mismatch sequence (Tombelli et al., 2000). Marrazza et al. (2000) used PCR coupled with chronopotentiometry to detect 4 mg/mL of ApoE mutant oligonucleotides. Guo et al. (2011) employed PNA–DNA interactions with Ni^{2+} ions to achieve 10 fM detection of ApoE target DNA. Work towards the integration of PCR amplification step with our sensor to detect ApoE gene mutations in real patient samples is currently under progress in our laboratory. The simplicity of the dual-detection method is promising towards the development of high-throughput miniaturized biosensors.

Acknowledgments

K.K. gratefully acknowledges the financial support from the Alzheimer Society of Canada and NSERC Discovery Grant. X.R.C. acknowledges the Alexander Graham Bell Canada Graduate Scholarship for Doctoral students from NSERC.

Appendix A. Supplementary material

Supplementary data associated with this article can be found in the online version at http://dx.doi.org/10.1016/j.bios.2013.10.003.

References

Ahmed, M.U., Idegami, K., Chikae, M., Kerman, K., Chaumpluk, P., Yamamura, S., Tamiya, E., 2007. Analyst 132, 431–438.
Anker, J.N., Hall, W.P., Lyandres, O., Shah, N.C., Zhao, J., Van Duyne, R.P., 2008. Nat. Mater. 7, 442–453.
Chang, B.-Y., Park, S.-M., 2010. Anal. Chem. 3, 207–229.
Cheng, W., Dong, S., Wang, E., 2002. Anal. Chem. 74, 3599–3604.
Claussen, J.C., Wickner, M.M., Fisher, T.S., Porterfield, D.M., 2011. ACS Appl. Mater. Interfaces 3, 1765–1770.
Corder, E., Saunders, A., Strittmatter, W., Schmechel, D., Gaskell, P., Small, G., Roses, A., Haines, J., Pericak-Vance, M., 1993. Science 261, 921–923.
de Bellis, G., Salani, G., Panigone, S., Betti, F., Invernizzi, L., Luzzana, M., 1997. Clin. Chem. 43, 1321–1324.
Endo, T., Kerman, K., Nagatani, N., Takamura, Y., Tamiya, E., 2005. Anal. Chem. 77, 6976–6984.
Endo, T., Kerman, K., Nagatani, N., Hiep, H.M., Kim, D.K., Yonezawa, Y., Nakano, K., Tamiya, E., 2006. Anal. Chem. 78, 6465–6475.
Endo, T., Kerman, K., Nagatani, N., Tamiya, E., 2007. J. Phys.: Condens. Matter 19, 5201–5210.
Endo, T., Yamamura, S., Kerman, K., Tamiya, E., 2008. Anal. Chim. Acta 614, 182–189.
Endo, T., Ikeda, D., Kawakami, Y., Yanagida, Y., Hatsuzawa, T., 2010. Anal. Chim. Acta 661, 200–205.
Farrer, L.A., Cupples, L.A., Haines, J.L., Hyman, B., Kukull, W.A., Mayeux, R., Myers, R.H., Pericak-Vance, M.A., Risch, N., van Duijn, C.M., 1997. J. Am. Med. Assoc. 278, 1349–1356.
Guo, K., Li, X., Kraatz, H.-B., 2011. Biosens. Bioelectron. 27, 187–191.
Grodzka, E., Pieta, P., Dluzewski, P., Kutner, W., Winkler, K., 2009. Electrochim. Acta 54, 5621–5628.
Haes, A.J., Van Duyne, R.P., 2002. J. Am. Chem. Soc. 124, 10596–10604.
Haes, A.J., Van Duyne, R.P., 2004. Anal. Bioanal. Chem. 379, 920–930.
Hezard, T., Fajerwerg, K., Evrard, D., Collière, V., Behra, P., Gros, P., 2012. J. Electroanal. Chem. 664, 46–52.
Hiep, H.M., Endo, T., Kerman, K., Chikae, M., Kim, D.-K., Yamamura, S., Takamura, Y., Tamiya, E., 2008a. Sci. Technol. Adv. Mater. 8, 331–338.
Hiep, H.M., Endo, T., Saito, M., Chikae, M., Kim, D.-K., Yamamura, S., Takamura, Y., Tamiya, E., 2008b. Anal. Chem. 80, 1859–1864.
Hiep, H.M., Kerman, K., Endo, T., Saito, M., Tamiya, E., 2010. Anal. Chim. Acta 661, 111–116.
Hsu, C.Y., Huang, J.W., Lin, K.-J., 2011. Chem. Commun. 47, 872–874.
Kim, D.-K., Kerman, K., Saito, M., Sathuluri, R.R., Endo, T., Yamamura, S., Kwon, Y.S., Tamiya, E., 2007. Anal. Chem. 79, 1855–1864.
Lahav, M., Gabai, R., Shipway, A.N., Willner, I., 1999. Chem. Commun., 1937–1938.
Lee, T.M.-H., Li, L.-L., Hsing, I.-M., 2003. Langmuir 19, 4338–4343.
Liang, G., Li, X., Liu, X., 2013. Biosens. Bioelectron. 48, 238–243.
Long, Y.-T., Li, C.-Z., Sutherland, T.C., Kraatz, H.-B., Lee, J.S., 2004. Anal. Chem. 76, 4059–4065.
Ma, Y.T., Di, J.W., Yan, X., Zhao, M.L., Lu, Z.J., Tu, Y.F., 2009. Biosens. Bioelectron. 24, 1480–1483.
Marrazza, G., Chiti, G., Mascini, M., Anichini, M., 2000. Clin. Chem. 46, 31–37.
Marrazza, G., Tombelli, S., Mascini, M., Manzoni, A., 2001. Clin. Chim. Acta 307, 241–248.
Merrick, D.M., Eminhizer, L.B., Villaume, J.F., 1973. Am. Mineral. 58, 920–925.
Morris, J.C., Roe, C.M., Xiong, C., Fagan, A.M., Goate, A.M., Holtzman, D.M., Mintun, M.A., 2010. Ann. Neurol. 67, 122–131.
Murphy, C.J., Gole, A.M., Hunyadi, S.E., Stone, J.W., Sisco, P.N., Alkilany, A., Kinard, B.E., Sakai, N., Fujiwara, Y., Arai, M., Yu, K., Tatsuma, T., 2009. J. Electroanal. Chem. 628, 7–15.
Paleček, E., Bartošík, M., 2012. Chem. Rev. 112, 3427–3481.
Randviir, E.P., Banks, C.E., 2013. Anal. Methods 5, 1098–1115.
Tombelli, S., Mascini, M., Braccini, L., Anichini, M., Turner, A.P.F., 2000. Biosens. Bioelectron. 15, 363–370.
Toyota, A., Nakashima, N., Sagara, T., 2004. J. Electroanal. Chem. 565, 335–342.
Venter, J.C., 2001. Science 291, 1304–1351.
Wang, L., Mao, W., Ni, D., Di, J., Wu, Y., Tu, Y., 2008. Electrochem. Commun. 10, 673–676.
Wang, Y., Deng, J., Di, J., Tu, Y., 2009. Electrochem. Commun. 11, 1034–1037.
Willets, K.A., Van Duyne, R.P., 2007. Annu. Rev. Phys. Chem. 58, 267–297.